Dynamic Modeling of the Reactive Twin-Screw Corotating Extrusion Process: Experimental Validation by Using Inlet Glass Fibers Injection Response and Application to Polymers Degassi...

ARTICLE *in* INDUSTRIAL & ENGINEERING CHEMISTRY RESEARCH · AUGUST 2012

Impact Factor: 2.59 · DOI: 10.1021/ie300698k

5 AUTHORS, INCLUDING:

Françoise Couenne
Claude Bernard University Lyon 1
71 PUBLICATIONS **369** CITATIONS
SEE PROFILE

Yann Le Gorrec
Institut Franche-Comté Electronique Mécani...
107 PUBLICATIONS **498** CITATIONS
SEE PROFILE

Generic Dynamic Model for Simulation and Control of Reactive Extrusion

S. Choulak,[†] F. Couenne,*[,†] Y. Le Gorrec,[†] C. Jallut,[†] P. Cassagnau,[‡] and A. Michel[‡]

Laboratoire d'Automatique et de Génie des Procédés, Université Claude Bernard, ESCPE, UMR CNRS 5007, Bat 308 G, 43 Bvd du 11 Nov 1918, 69622 Villeurbanne Cedex, France, and Laboratoire des Matières Plastiques et des Biomatériaux, Université Claude Bernard, ISTIL, UMR CNRS 5627, 43 Bvd du 11 Nov 1918, 69622 Villeurbanne Cedex, France

A one-dimensional physically motivated dynamic model of a twin-screw extruder for reactive extrusion has been developed. This model predicts the transient and stationary behavior of the extruder for pressure, filling ratio, temperature, and molar conversion profiles as well as residence time distribution under various operating conditions. The model consists of a cascade of perfectly stirred reactors that can be either fully filled with backflow or partially filled according to the operating conditions. Each reactor is described by the reactant concentrations and the melt temperature. A piece of barrel and screw, described by their temperature, is associated with each reactor. Living polymerization of ϵ-caprolactone with tetrapropoxytitanium as the initiator is chosen as an example of application. The flow representation aspect of the model is validated by using experimental residence time distributions. Validation of the model is derived from simulation results as well as comparison with experimental data.

Introduction

A growing interest has emerged in using twin-screw extruders as continuous chemical reactors for the polymerization. The main specific properties of the synthesized polymer are intrinsically linked to the operating pressure and temperature. The primary objective of our research is the automatic control of polymerization conditions in a twin-screw corotating extruder. As a first step to achieving this goal, we propose a dynamic model of the extrusion process. This model has to represent all of the dynamic relations between the controlled variables and the manipulated ones. Considering the highly nonlinear behavior of the process and the coupling between the variables, a knowledge-based model is necessary in order to capture the main phenomena associated with the reactive extrusion process.

As far as we know, control laws for extrusion processes are based on oversimplified or empirical models. This approach gives rise to the synthesis of very conservative control laws because of the uncertainty of the models.[1−6] Clearly, the automatic control of such processes needs to have a good understanding of mass flow, rheology, mixing time, and thermal behavior.

Highly detailed models are available in the literature. They are based on a one-dimensional (1D) representation of the flow[7−12] or on the residence time distribution (RTD) representation.[13,14] Such models are not relevant for process control because they are stationary models.

Four interesting papers emerge in food engineering:[15−18] In these papers are proposed models for a twin-screw corotating extruder taking into account mass and energy balances. The two first papers propose stationary models.

In refs 18 and 17 are presented a model for extrusion cooking based on heat and material balances of the melt. The flow is divided into two zones: a partially filled (PF) one and a completely filled (CF) one separated by a moving boundary. The authors obtain models described by partial differential equations for the temperature and mass flow rate with algebraic constraints for the pressure in the CF zone. Although these models are an interesting basis, the manipulated variables for the control of an extruder are not generally used as input variables: for example, in ref 17, the barrel temperature is fixed.

Finally, almost all of the authors give models under some restrictive assumptions because many phenomena occur in the extruder. All of the authors consider 1D analysis. This hypothesis is reasonable according to the geometry of the system. The model we build up is also unidirectional.

The second aspect of the models available in the literature is connected with the description of flows along the extruder. To some extent, the presented models are based on some fixed structure of the flow with respect to the filling ratio along the extruder. In this paper, we present a more flexible model in the sense that the PF and the CF zones are not predefined. Simulation can be performed from an initial state corresponding to an empty extruder. Such a simulation is possible by adapting a spatially discretized version of the 1D representation.

The modeling objective is to predict not only the temperature of the melt but also that of the barrel, concentration, and pressure profiles at any time and for a large class of input variables (feed rate, composition, screw speed, and heat flux supplied to the barrel). These variables are the manipulated variables for operating the extrusion process. In that sense, the model that we present is well adapted for automatic control. Moreover, the computation time on a 1.5-GHz personal computer for the simulation of our model performed with MATLAB is compatible with control purposes.

* To whom correspondence should be addressed. Tel.: 33 4 72 43 18 82. Fax: 33 4 72 43 16 82. E-mail: couenne@lagep.univ-lyon1.fr.

[†] Laboratoire d'Automatique et de Génie des Procédés, Université Claude Bernard.

[‡] Laboratoire des Matières Plastiques et des Biomatériaux, Université Claude Bernard.

10.1021/ie0342964 CCC: $27.50
Published on Web 10/06/2004

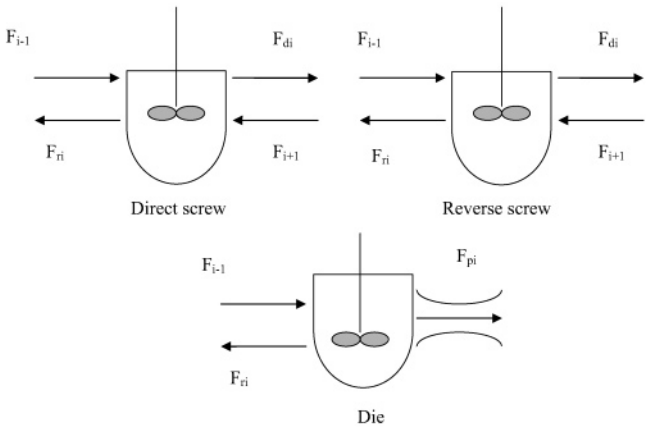

Figure 1. Structures of the basic elements.

In the next section, the model used to describe the different phenomena occurring in the reactive extrusion process, the simulation algorithm, and the method to adjust some parameters from the experimental RTD are presented. Simulation results are given in the following section, and finally qualitative validation is presented and discussed.

Description of the Model

Introduction. In this section, the main equations describing the model are set up. The model is based on the fact that the flow of matter can be seen as a cascade of continuous stirred tank reactors (CSTRs) with possible backflows. The flow rate expressions are based on the geometry of the screw. A piece of barrel and a piece of screw are associated with each CSTR. We will see in the next section that one of the degrees of freedom to fit the model is the number of reactors.

Flow Modeling: an Arrangement of Basic Elements. The CSTR model with backflow is chosen as the basic element of the model. It can be compared to the generalized C-chamber model used in ref 14. A second kind of element is necessary to represent the die and interconnection between direct and reverse screw elements. This second element is a Poiseuille flow inside a tube. Finally, by a suitable arrangement of such basic elements, one can represent any element of the screw (direct-screw elements, reverse-screw elements, the kneading disk block, and the die). The kneading disk block can be considered as a direct-screw element or a reverse one according to the staggering angle. These basic elements are presented in Figure 1: they correspond to the die, a piece of the reverse screw, and a piece of direct screw. As mentioned before, the Poiseuille element is used to build the die element as well as to connect the direct and reverse pieces of the screw.

These reactors are characterized by their free volume V_i and mass flows: (i) mass flows representing the net flows coming from the reactors indexed by $i - 1$ and $i + 1$; (ii) those directly due to reactor i: F_{di}, F_{ri}, and in some cases the Poiseuille flow F_{pi}.

In Figure 2, a simple example of serial arrangement is given where each screw element is represented by only one CSTR. The screw is made of a series of one direct screw (1d), a reverse one (2r), a direct one (3d), and finally the die (4die). A Poiseuille flow is placed between the direct- and reverse-screw elements because without this term the upstream reactor, but not the downstream one, can be filled up.[19]

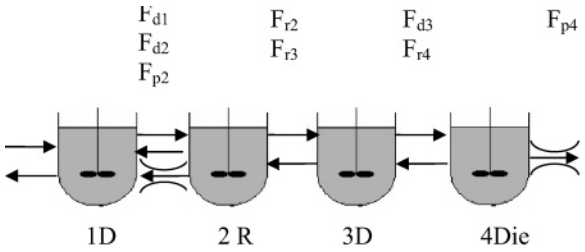

Figure 2. Example of the arrangement of the basic elements.

Table 1. Expressions of Flow Rates

reactor i	F_{di}	F_{ri}, F_{pi}	
direct pitch	$K_{di}Nf_iV_i$	$\frac{K_{ri}}{\eta_i}(P_i - P_{i-1})$	
reverse pitch	$K_{di}Nf_iV_i$	$\frac{K_{ri}}{\eta_i}(P_i - P_{i+1})$,	$\frac{K_{pi}}{\eta_i}(P_i - P_{i-1})$
die		$\frac{K_{rn}}{\eta_n}(P_n - P_{n-1})$,	$\frac{K_{pn}}{\eta_n}(P_n - P_a)$

There is no pressure buildup in a PF reactor, and then only the direct flow F_{di} appears. In a CF reactor i, the filling ratio f_i (the ratio of the volume occupied by the matter to the free volume) is equal to 1; there is a pressure gradient, and then a reverse flow F_{ri} occurs. Moreover, the total mass balance becomes algebraic.

The total mass balance for reactor i is then given by

$$\begin{cases} \rho V_i \dfrac{\mathrm{d}f_i}{\mathrm{d}t} = F_{i-1} + F_{i+1} - F_{di} & \text{if } f_i < 1 \\ 0 = F_{i-1} + F_{i+1} - F_{di} - F_{ri} - F_{pi} & \text{if } f_i = 1 \end{cases} \quad (1)$$

and for the die

$$\begin{cases} \rho V_n \dfrac{\mathrm{d}f_n}{\mathrm{d}t} = F_{n-1} & \text{if } f_n < 1 \\ 0 = F_{n-1} - F_{pn} - F_{rn} & \text{if } f_n = 1 \end{cases} \quad (2)$$

Expressions of the direct and reverse flow rates are available in ref 20: they correspond to a simplified 1D model of the flow.[9−12] The expressions of these flow rates depend on the screw configuration. They are given in Table 1.

The constant parameters K_{di} and K_{ri} are functions of the geometry of the screw and of the length of the piece of screw under consideration as described in ref 20. The melt viscosity η_i is calculated according to the state of the melt in reactor i. Its expression is given in the Appendix.

At this stage, the material and energy balances have to be established for a basic CSTR element. This will be done in the next section.

Material and Energy Balances. Figure 3 gives a schematic representation of the extruder on the basis of the cascade of reactors. With each of these reactors is associated a piece of barrel and screw. The temperature of these elements is assumed to be uniform.

We will consider the case when only one reaction occurs in the extruder, leading to the consumption of a monomer in the presence of a species that is neither consumed nor produced, like an initiator. We will detail the mass balance for the initiator and monomer. The total mass balance is given in eq 1 with the rough approximation that the mean melt density ρ is constant. So, the mass fractions of the initiator and monomer in

reactor i are respectively given by

$$w_i^{\mathrm{I}} = \frac{\mathscr{M}^{\mathrm{I}} n_i^{\mathrm{I}}}{\rho V_i f_i}, \quad w_i^{\epsilon} = \frac{\mathscr{M}^{\epsilon} n_i^{\epsilon}}{\rho V_i f_i}$$

The initiator mass balance (superscript I) is given by

$$\mathscr{M}^{\mathrm{I}} \frac{\mathrm{d}n_i^{\mathrm{I}}}{\mathrm{d}t} = (w_{i-1}^{\mathrm{I}} F_{i-1} + w_{i+1}^{\mathrm{I}} F_{i+1}) - w_i^{\mathrm{I}}(F_{\mathrm{d}i} + F_{\mathrm{r}i}) \quad (3)$$

In a same way, the monomer mass balance (superscript ϵ) is given by

$$\mathscr{M}^{\epsilon} \frac{\mathrm{d}n_i^{\epsilon}}{\mathrm{d}t} = (w_{i-1}^{\epsilon} F_{i-1} + w_{i+1}^{\epsilon} F_{i+1}) - w_i^{\epsilon}(F_{\mathrm{d}i} + F_{\mathrm{r}i}) - \mathscr{M}^{\epsilon} r_i f_i V_i \quad (4)$$

where r_i is the molar reaction rate.

Let us now write the energy balance of the melt in reactor i:

$$f_i M_i^{\mathrm{m}} C_{\mathrm{p}}^{\mathrm{m}} \frac{\mathrm{d}T_i^{\mathrm{m}}}{\mathrm{d}t} = F_{i-1} C_{\mathrm{p}}^{\mathrm{m}}(T_{i-1}^{\mathrm{m}} - T_i^{\mathrm{m}}) + F_{i+1} C_{\mathrm{p}}^{\mathrm{m}}(T_{i+1}^{\mathrm{m}} - T_i^{\mathrm{m}}) + \alpha_{\mathrm{b}} f_i S_{\mathrm{b}}(T_i^{\mathrm{b}} - T_i^{\mathrm{m}}) + \alpha_{\mathrm{s}} f_i S_{\mathrm{s}}(T_i^{\mathrm{s}} - T_i^{\mathrm{m}}) + f_i \Psi_i + (-\Delta H) f_i V_i r_i \quad (5)$$

The two first terms on the right-hand side of the equality represent the energy convected by the flowing matter. The specific heat capacity of the melt is supposed to be constant. The third and forth terms represent the heat transfer between the melt and the barrel and the heat transfer between the melt and the screw. The two last terms correspond to the viscous heat dissipation and the heat flux due to the reaction.

In a same way, the energy balance of the associated pieces of barrel and screw is given by

$$M_i^{\mathrm{b}} C_{\mathrm{p}}^{\mathrm{b}} \frac{\mathrm{d}T_i^{\mathrm{b}}}{\mathrm{d}t} = \alpha_{\mathrm{e}} S_{\mathrm{e}}(T_{\mathrm{e}} - T_i^{\mathrm{b}}) + \alpha_{\mathrm{b}} f_i S_{\mathrm{b}}(T_i^{\mathrm{m}} - T_i^{\mathrm{b}}) + \frac{\lambda_{\mathrm{b}} s^{\mathrm{b}}}{e_{i-1}}(T_{i-1}^{\mathrm{b}} - T_i^{\mathrm{b}}) + \frac{\lambda_{\mathrm{b}} s^{\mathrm{b}}}{e_i}(T_{i+1}^{\mathrm{b}} - T_i^{\mathrm{b}}) + \Phi_i \quad (6)$$

This eq 6 describes the heat transfer between the surroundings and the barrel and the heat transfer between the polymer melt and the barrel.[19−21] Moreover, longitudinal thermal conduction is considered in the barrel. The last term represents the heat flux due to electrical resistance heaters. Finally, the energy balance on the associated piece of screw is given by

$$M_i^{\mathrm{s}} C_p^{\mathrm{s}} \frac{\mathrm{d}T_i^{\mathrm{s}}}{\mathrm{d}t} = \alpha_{\mathrm{s}} f_i S_{\mathrm{s}}(T_i^{\mathrm{m}} - T_i^{\mathrm{s}}) + \frac{\lambda_{\mathrm{s}} s^{\mathrm{s}}}{e_{i-1}}(T_{i-1}^{\mathrm{s}} - T_i^{\mathrm{s}}) + \frac{\lambda_{\mathrm{s}} s^{\mathrm{s}}}{e_i}(T_{i+1}^{\mathrm{s}} - T_i^{\mathrm{s}}) \quad (7)$$

Again longitudinal thermal conduction is considered in the screw.

Simulation Algorithm. Considering the aforementioned elements of modeling, it is possible to derive an efficient algorithm to help the designer in the modeling.

Step 0. The computation process is initiated by fixing profiles of the filling ratio, concentration, and temperature along the extruder. Usually the extruder is considered to be initially empty, i.e., $f_i = 0, \forall\, i$.

Step 1. The computation of direct flow rates is done. The profile of pressure is deduced from algebraic equations (1) and/or (2). To that end, we have to solve a linear system of the type $\mathbf{AP} = \mathbf{B}$, where $\mathbf{A}$ is an $n \times n$ matrix, $\mathbf{B}$ a vector, and $\mathbf{P}$ the pressure profile vector. The matrix $\mathbf{A}$ is tridiagonal and always regular (see the Appendix).

Step 2. The differential equations (1) and (2) can be integrated. At this stage, it can be emphasized that it must be decided if the CF zone remains completely filled or not. This is decided by checking if the pressure is greater than the atmospheric pressure. If it is smaller, then eq 1 or 2 is governed by the differential equation. The reverse flow F_{ri} is deduced.

Step 3. All of the differential equations (3)−(7) governing the process are integrated.

Model Adjustment. Let us consider that, for a given screw profile, one discretizes the flow by a serial arrangement of N_{c} CSTRs and Poiseuille flow elements. The model is then able to calculate the time evolutions of the pressure profile, the filling ratio profile, and the RTD, provided that the expressions of the parameters K_{ri}, K_{di}, and $K_{\mathrm{p}i}$ as given in ref 20 (see Table 1) are sufficiently accurate. In the sequel, this version of the model will be designated as the *geometrical model*.

However, these expressions correspond to an oversimplified model of the flow. Furthermore, the model accuracy depends on the level of discretization corresponding to the number of CSTRs. From a control point of view, one has interest to minimize this number.

Consequently, a parameter estimation may be performed to find the best combination of N_{c}, K_{ri}, K_{di}, and $K_{\mathrm{p}i}$. In this paper, we have used experimental RTDs in order to perform such an estimation. This model is then designated as the *identified model*.

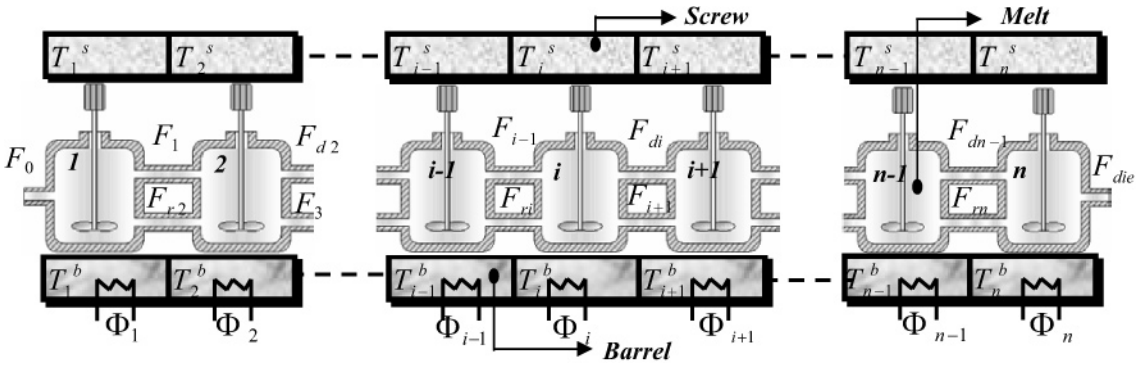

Figure 3. Cascade representation of the extruder.

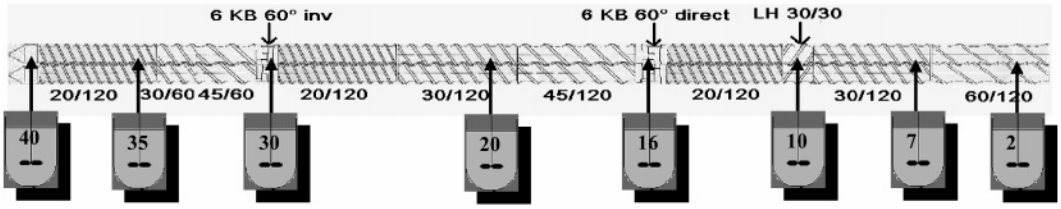

Figure 4. Profile of the screw and the distribution of the reactors.

Experimental RTDs are performed at steady-state conditions. For a given set of parameters and for the corresponding operation conditions, the model is able to predict the steady-state flow arrangement. From this point, the theoretical response of the system to the injection of an inert tracer is calculated and compared to the experimental RTD. This comparison allows parameter adjustment.

Simulation Example

Introduction. The reaction under consideration is the living polymerization of ϵ-caprolactone with tetrapropoxytitanium as the initiator. All of the physicochemical parameters (rheological properties, reaction rate, enthalpy, etc.) concerning this reaction can be found in refs 22−24. As specified in ref 22, we consider that the reaction rate is of order 1 with respect to the monomer. Its expression is given by

$$r_i = k\left(\frac{n_i^{\mathrm{I}}}{\rho V_i f_i}\right)^{\alpha} \mathrm{e}^{-E/RT_i^{\mathrm{m}}} n_i^{\epsilon} \frac{1}{f_i V_i} \tag{8}$$

The polymerization is supposed to be carried out in an intermeshing self-wiping corotating extruder (Leistritz LSM 30-34; centerline distance, $C_1 = 30$ mm; screw diameter, $D = 34$ mm; barrel length, $L = 1.2$ m). The extruder barrel is divided into 10 equal zones. Each zone has individual electrical resistance heaters and water cooling systems. The screw profile is made up of two blocks of kneading disks, one direct screw (right-handed elements), one reverse screw (left-handed elements), and the die. The tubular die is 10 mm long, and its diameter is 2 mm.

Figure 4 gives the screw profile used all along this paper and the number of reactors associated with each peace of screw. In this figure, one can see, according to the flow direction, a direct element zone followed by a reverse element (reactor 10), a direct element, a kneading block (reactor 16), a direct element, another kneading block (reactor 30), and the die (reactor 40).

Experimental Validation of the Flow Modeling. RTD experiments have been carried out using an inline UV fluorescence method. They have been performed with polypropylene because the polypropylene viscosity characteristics are close to the polycaprolactone characteristics. The estimation procedure uses the experimental RTD obtained for $N = 150$ rpm and $F_0 = 5$ kg·h^{-1} (see Figure 5).

From that point, RTD experiments are simulated under other operating conditions without any further estimation procedure. In Figures 6 and 7, we compare the experimental RTDs with the identified model as well as the *geometrical model*. The characteristics of the *geometrical model* are as follows:

(i) The number and volume of the CSTRs are the same as those of the identified model.

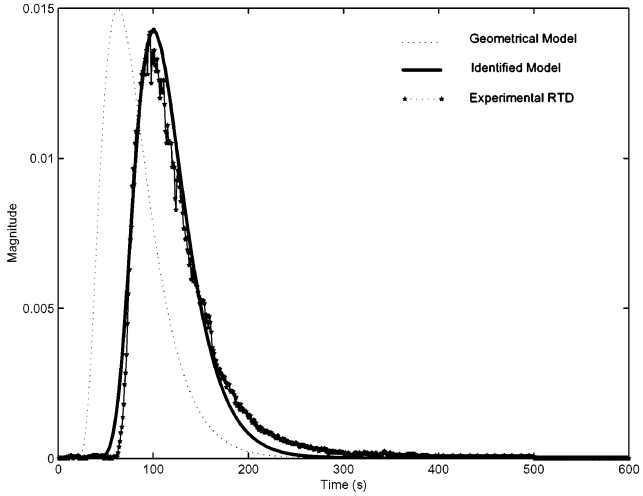

Figure 5. RTD at a screw speed of 150 rpm and a flow rate of 5 kg·h^{-1}.

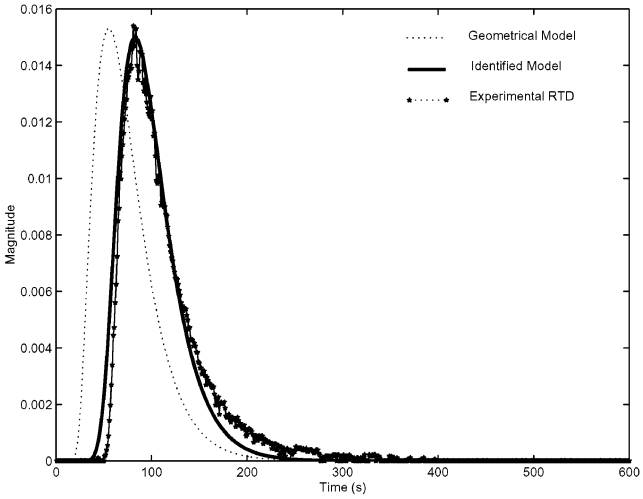

Figure 6. RTD at a screw speed of 200 rpm and a flow rate of 5 kg·h^{-1}.

(ii) The direct and reverse flows are calculated by using equations given in Table 1 and the geometrical values for the parameters as given in ref 20.

Figure 6 presents a RTD at a screw speed of 200 rpm and at a flow rate of 5 kg·h^{-1}.

Figure 7 presents a RTD at a screw speed of 160 rpm and at a flow rate of 8 kg·h^{-1}.

Although the melting zone for polypropylene is not taken into account, the identified model is satisfactory because the time delay as well as the shape of the RTD is well-fitted. Moreover, the identified model is closer to the RTD experiments than the geometrical one. It can be seen that this geometrical model is less satisfactory because of the lack of precision of the parameter appearing in the expressions given in Table 1. The order of magnitude of the direct and reverse flows is good, but

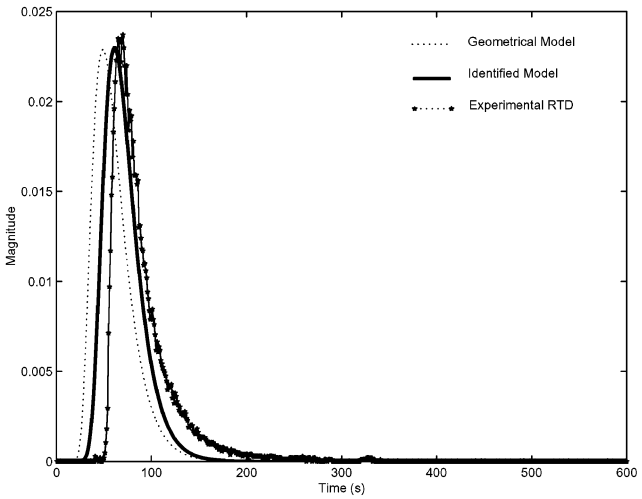

Figure 7. RTD at a screw speed of 160 rpm and a flow rate of 8 kg·h^{-1}.

one has to correct their theoretical predictions from the fitting results.

Clearly, the models have good trends from the RTD point of view. In the next section, simulation results for the evolution of temperature, concentration, viscosity, and pressure for steps of screw speed, input ratio M_0/I_0, and inlet flow rate are presented.

Simulation Results. First of all, let us notice that these simulation results are made by assuming that any regulation on the barrel temperature is performed. We only apply a constant heat power to each barrel zone.

(i) Steady-State Profiles. In Figures 8 and 9, caprolactone monomer conversion and viscosity profiles are shown for various monomer/initiator inlet ratios and for various screw speeds.

In Figure 8a, monomer conversion profile increases with the screw length and is always equal to 100% at the outlet. The higher the ratio M_0/I_0 is, the lower the conversion increase is because of the reaction rate equation (8). Because of the evolution of the viscosity with M_0/I_0 (see eq 11 or 12 in the Appendix), for a low value of M_0/I_0, the viscosity increases more rapidly, but its value is lower at the outlet as shown in Figure 8b.

In Figure 9, the same kind of behavior can be seen for different screw speeds. Moreover, in Figure 9b, a rapid rise of the viscosity around the position 0.8 m, which corresponds to the position of an inverse screw, can be seen. This induces a bigger residence time at this position, an increase of the conversion, and then an increase of the viscosity.

An increase of the screw speed leads to an increase of the melt temperature by viscous heat dissipation and to a reduction of the residence time. Thus, these two effects make the analysis of the reaction more difficult. An increase of the melt temperature tends to an increase of the conversion, but a reduction of the residence time tends to a decrease of this conversion. In Figure 9a, it is seen that the conversion decreases when the screw speed increases. In Figure 9b, a drop of the viscosity can be observed with an increase of the screw speed.

However, the strength of this model lies in its ability to simulate transient phenomena.

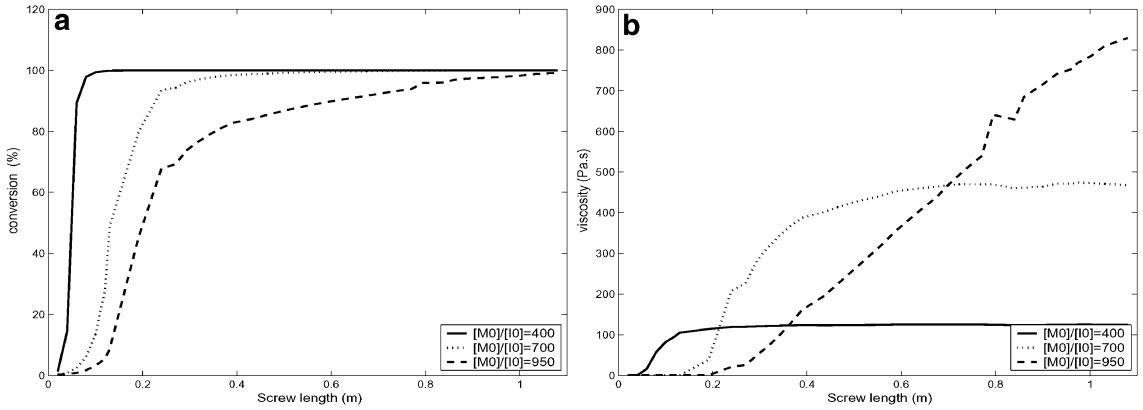

Figure 8. (a) Conversion profile for different ratios M_0/I_0. (b) Viscosity profile for different ratios M_0/I_0 for $F_0 = 3$ kg·h^{-1} and $N = 100$ rpm.

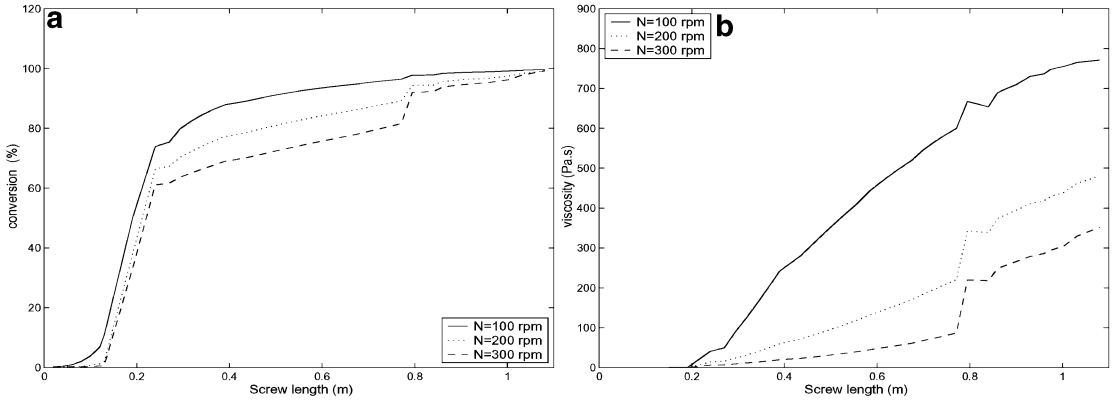

Figure 9. (a) Conversion profile for different screw speeds. (b) Viscosity profile for different screw speeds for $F_0 = 3$ kg·h^{-1} and $M_0/I_0 = 400$.

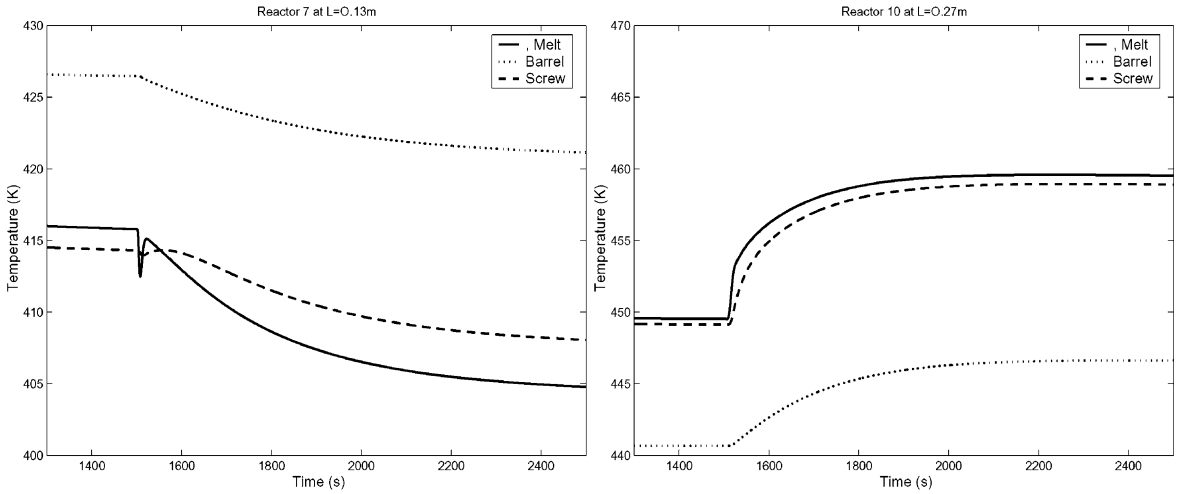

Figure 10. Temperatures vs time in reactors 7 and 10 for a flow rate step change.

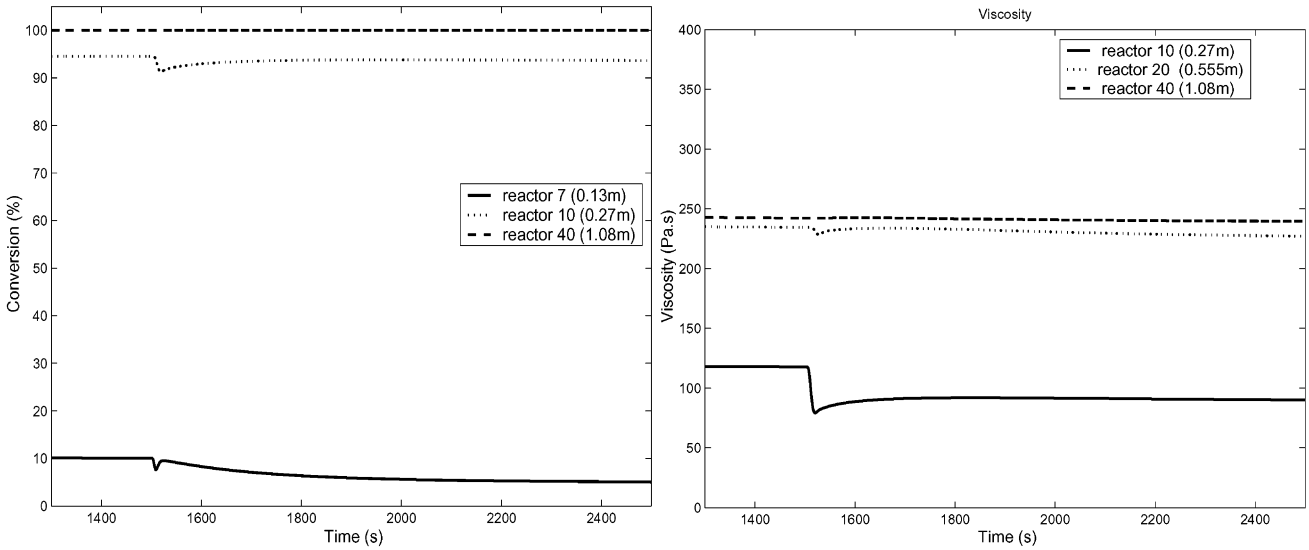

Figure 11. Conversion in reactors 7, 10, and 40 and viscosity versus time in reactors 10, 20, and 40 for a flow rate step change.

(ii) Transient Simulation: Response to a Step Change in the Inlet Flow Rate. In this set of simulation results, we will present dynamical effects along the extruder for an inlet flow rate step from $F_0 =$ 3 to 6 kg·h^{-1} occurring at $t = 1500$ s. This is exemplified by considering the temperature in reactors 7 and 10 (Figure 10) for the initial conditions $T_i^b = 433$ K, $T_i^s =$ 400 K, and $T_i^m = 398$ K and the operating conditions N = 200 rpm and $M_0/I_0 = 600$. The electrical power applied to the elements of the barrel is 8.8 kW·m^{-1}.

Reactor 7 represents a direct-screw element, which is PF in these conditions, and reactor 10 represents the first inverse element in the extruder.

As can be seen in reactor 7, the temperature of the melt decreases in the zone close to the extruder inlet: this is due to the increase of the flow. From reactor 7, the screw and the matter are almost at the same temperature. From reactor 10, there is a significative increase of the melt temperature. This is mainly due to the heat of reaction.

This increase of temperature then induces a decrease of the viscosity. It is perfectly visible in Figure 11 in reactor 10 because the conversion is very important in this reactor (the inverse-screw element). In reactors 20 and 40, this effect is no more visible because the monomer is totally converted as shown also in Figure 11.

(iii) Transient Simulation: Response to a Step Change in the Monomer Initiator Inlet Ratio. We present dynamical effects along the extruder for a monomer initiator inlet ratio step from 400 to 800 occurring at $t = 1500$ s. The initial conditions are $T_i^b =$ 433 K and $T_i^s = 400$ K, and the operating conditions are $F_0 = 3$ kg·h^{-1} and $N = 200$ rpm. The weight-average molecular weight M_w and viscosity are given in Figure 12.

The general tendency to this step change is the increase of M_w except in the zone close to the extruder inlet. The other effect of this step change is the decrease of the initiator concentration and then the decrease of the reaction rate.

In the upstream PF reactors, the decrease of the reaction rate is important. So, a fall of M_w is noticed, as shown in Figure 12, at reactor 5. At reactor 10, the reaction increases, so M_w increases.

The influence of the ratio M_0/I_0 is similar to that pointed out in the case of the steady-state simulations.

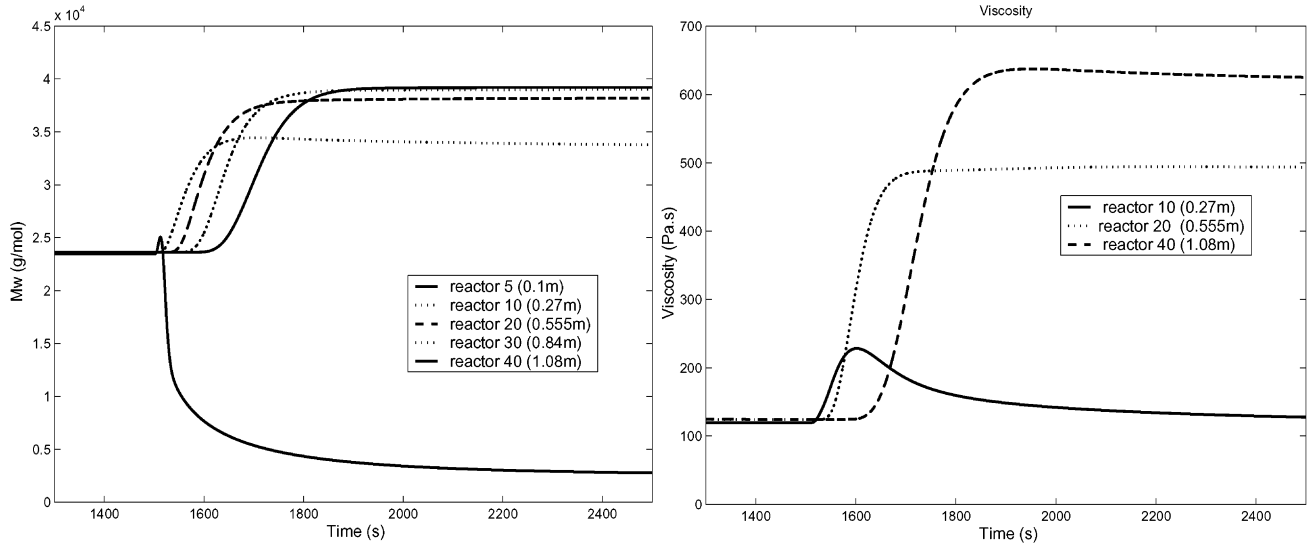

Figure 12. M_w and viscosity versus time in some reactors for a step change of the monomer initiator ratio.

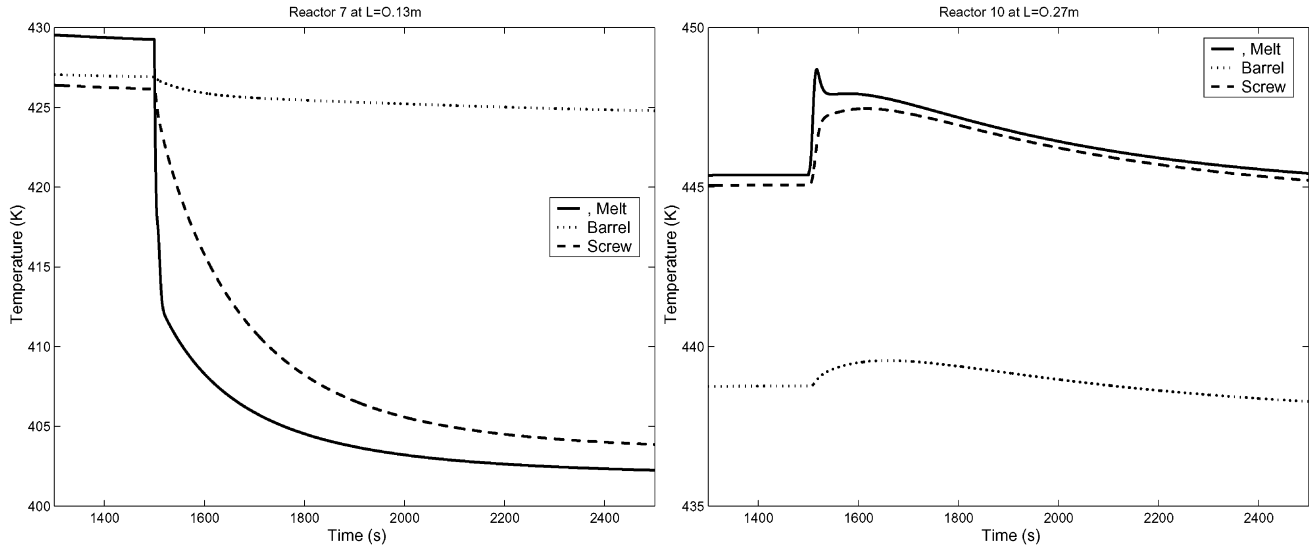

Figure 13. Temperatures vs time in reactors 7 and 10 for a step change of the screw speed.

At the beginning, an increase of the ratio corresponds to a decrease of the reaction rate and consequently of the viscosity. However, at the die, the viscosity is higher because the polymer chains are longer.

(iv) Transient Simulation: Response to a Step Change in the Screw Speed. We present dynamical effects along the extruder for a step change in the screw speed from 100 to 250 rpm occurring at $t = 1500$ s. Again we analyze the temperature behavior in the extruder. The operating conditions are $F_0 = 3$ kg·h^{-1}, $M_0/I_0 = 600$, $T_i^b = 433$ K, and $T_i^s = 400$ K. The results are shown in Figure 13.

The residence time in the reactors decreases, which implies a smaller contact time between the melt and the barrel and so a temperature drop on the first reactors, as shown in Figure 13. On the other hand, the increase of speed implies an increase of the viscous heat dissipation (proportional to N^2). An overheating of the melt, which appears from reactor 10 (inverse-screw element), follows.

Two antagonistic effects appear on the conversion and viscosity, which give transitory peaks. First the increase of speed induces a decrease of the residence time and so a decrease of the conversion and of the temperature. This fall is then compensated for by the increase of the viscous heat dissipation. Because these two actions do not have the same magnitude, the final level is different from the initial one. This effect can be seen in Figure 14.

At the level of the die, the peak in the viscosity is no more visible because the conversion is complete: this means that the viscosity reaches its maximal value.

Experimental Validation

In this section, we present experimental results that can be found in ref 9 and we compare them with the pressure simulations at the die.

The first experiment is the transient response to a step change of speed. The operating conditions for this experiment are $M_0/I_0 = 1000$, $N = 105$ rpm, and $F_0 = 3$ kg·h^{-1}, and the initial condition is $T_i^b = 373$ K.

For a screw speed $N = 200$ and 300 rpm, the nuclear magnetic resonance analysis has shown that the stationary conversion is total.

Figure 15a gives the pressure response at the die to a step increase of 200−300 rpm at time $t = 485$ s. An

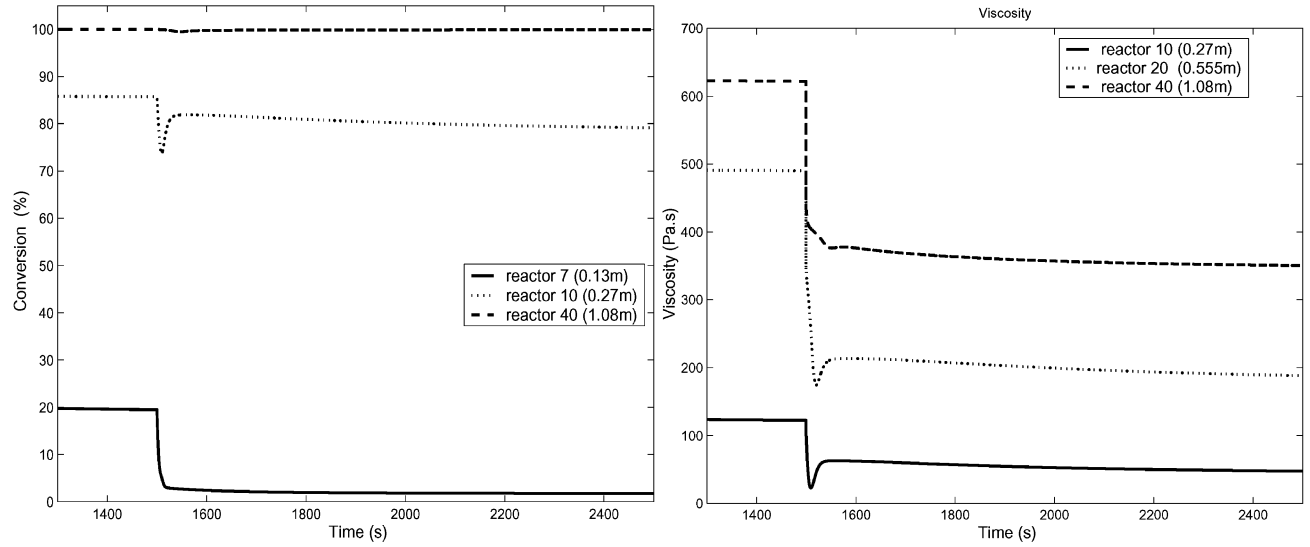

Figure 14. Conversion vs time in reactors 7, 10, and 40 and viscosity in reactors 10, 20, and 40 for a step change of the screw speed.

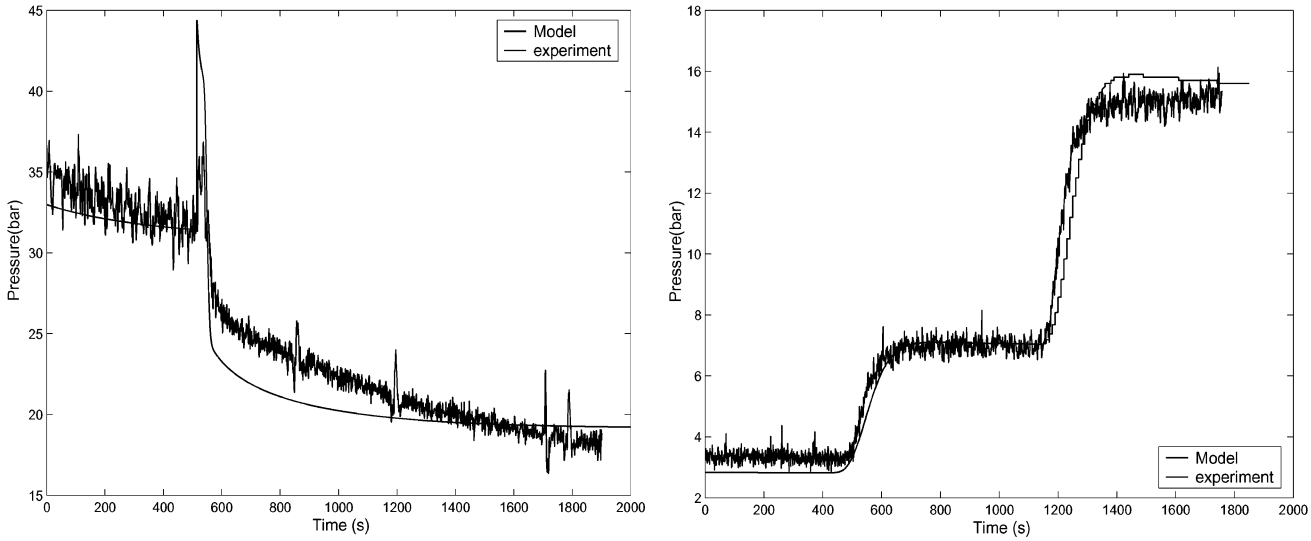

Figure 15. Pressure vs time at the die (a) for a step change of the screw speed and (b) for two step changes of M_0/I_0.

instantaneous increase of the pressure is shown because, for the process, it corresponds to an instantaneous increase of the output flow rate. Then it is followed by a decay explained by the change of the viscosity. Because the flow rate has not changed, the steady state is established at a lower pressure than that initially because the viscosity is lower.

The second comparison concerns the die pressure step response to monomer initiator inlet ratio. For this experiment, T_b is fixed at 433 K without temperature regulation, $N = 106$ rpm, and $F_0 = 3$ kg·h^{-1}. With such operating conditions, the conversion of the monomer is 100%. The first step change occurs at time $t = 350$ s from $M_0/I_0 = 400$ to 600 and the second one at time $t = 1035$ s from $M_0/I_0 = 600$ to 800.

From Figure 15b, it can be seen that the step of M_0/I_0 noticeably increases the die pressure. This is only due to the increase of the weight-average molecular weight.

These two results give us encouraging signs that this model can be used for simulation and automatic control purposes.

Conclusion

The methodology we have proposed for the extruder dynamic modeling gives encouraging results. As far as we know, the presented model is the first dynamic model for reactive extrusion that permits one to simulate the filling and the emptying of the extruder and also to give all of the profiles of temperature, pressure, and concentration along the time. The model is able to reproduce the main transient effects and the steady-state one occurring during reactive extrusion. Moreover, some simulations presented in the previous sections are qualitatively corroborated by experimental transient phenomena.

This model can be easily improved by choosing another arrangement of the CSTRs and by improving the accuracy of the expression used for the flow rate calculation. Moreover, a thermal study of the extruder would give us some additional information on the flow as well as heat-transfer coefficients.

At this stage, this model can also be used for automatic control purposes or supervision because the main

coupling between phenomena is taken into account and the model is related to the manipulated variables. Moreover, the computation time for the simulation of this model is not an obstacle for real-time control of this process.

Acknowledgment

The presented work has received support from the French National Center for Scientific Research (CNRS) under Project "Program Matériaux, Extrusion Réactive".

Appendix

Regularity of the Matrix A. In general, the screw profile is such that the CF zone is quite well located at more or less one reactor. So, the matrix **A** contains a diagonal term 1 for the PF reactor and has, in general, a tridiagonal structure in zones with CF reactors. To show that the matrix **A** is regular, let us check it in the following situation. Let us consider the profile with the following choice of zones: two with direct pitches, one with reverse pitch, and one with direct pitch. The filling ratio vector at the current time is $\mathbf{f}^{\mathrm{T}} = (f_1, 1, 1, f_4)$. It follows that the vector pressure $\mathbf{P}^{\mathrm{T}} = (P_1, P_3, P_3, P_4)$ is governed by

$$\mathbf{A} = \begin{bmatrix} 1 & 0 & 0 & 0 \\ K_{\mathrm{r2}} & -K_{\mathrm{r2}} - K_{\mathrm{p3}} & K_{\mathrm{p3}} & 0 \\ 0 & K_{\mathrm{p3}} & -K_{\mathrm{p3}} - K_{\mathrm{r3}} & K_{\mathrm{r3}} \\ 0 & 0 & 0 & 1 \end{bmatrix} \tag{9}$$

This situation is the most complicated one and leads to a regular matrix because the parameters $K_{\mathrm{p}i}$ and $K_{\mathrm{r}i}$ are positive and different from 0. So, we conclude that **A** is always a regular matrix.

Expression of the Rheological Properties. All of the expressions we use are precisely described in refs 22 and 23. Two types of flow regimes are considered. The melt at the beginning of the reaction is fluid, and as the reaction occurs, the melt becomes very viscous. The flow regime evolves from a Rouse regime to an entangled one. The transition between the two regimes depends on the critical entanglement molar weight and the conversion of polymer.

In the Rouse regime, we have a Newtonian behavior, which means that the viscosity does not depend on the shear rate. In the entangled regime, the evolution of the viscosity is given by a Carrau−Yasuda law.

The weight-average molecular weight is given by

$$\bar{M}_{\mathrm{w}i} = K_{\mathrm{c1}}(M_0/I_0)\tau_i + \mathscr{M}^{\epsilon} \tag{10}$$

where τ_i is the conversion.

From this point, for simplicity, we omit the index i representing the number of the reactor under consideration.

If the weight-average molecular weight is less than 2 times the entanglement molecular weight ($\bar{M}_{\mathrm{w}} < 2M_{\mathrm{e}}\tau^{-1.25}$), the Rouse regime is applied and the viscosity is given by

$$\eta = f_{\mathrm{Rouse}}(\tau, T^{\mathrm{m}}) = 2.24 \times 10^{-5} \exp\left(\frac{-E_{\mathrm{bs}}}{RT^{\mathrm{m}}}\right) \exp\left[\frac{E_{\mathrm{a}}}{R}\left(\frac{1}{T^{\mathrm{m}}} - \frac{1}{T_0}\right)\right] \tau \bar{M}_{\mathrm{w}}^{1/2} \tag{11}$$

For the entangled regime ($\bar{M}_{\mathrm{w}} > 2M_{\mathrm{e}}\tau^{-1.25}$), we have

$$\eta = f_{\mathrm{ent}}(\tau, T^{\mathrm{m}}) = \frac{\eta_0}{[1 + (\lambda\dot{\gamma})^a]^{(1-n)/a}} \tag{12}$$

with

$$\eta_0 = 1.35 \times 10^{-17} \exp\left(\frac{-E_{\mathrm{bs}}}{RT^{\mathrm{m}}}\right) \exp\left[\frac{E_{\mathrm{a}}}{R}\left(\frac{1}{T^{\mathrm{m}}} - \frac{1}{T_0}\right)\right] \tau^4 \bar{M}_{\mathrm{w}}^{4.4}$$

and

$$\lambda = 1.17 \times 10^{-20} \exp\left(\frac{-E_{\mathrm{bs}}}{RT^{m}}\right) \exp\left[\frac{E_{\mathrm{a}}}{R}\left(\frac{1}{T^{\mathrm{m}}} - \frac{1}{T_0}\right)\right] \tau^{1.75} \bar{M}_{\mathrm{w}}^{4.1}$$

where a = parameter characterizing the breadth of the transition region, E_{a} = flow activation energy, E_{bs} = difference of energy activation between a pure polymer and a polymer in solution, K_{c1} = parameter depending on M_0/I_0, M_{e} = entangled molecular weight, $\bar{M}_{\mathrm{w}}$ = weight-average molecular weight, n = pseudoplastic rating, R = molar gas constant, T_0 = reference temperature, η_0 = viscosity at zero shear rate, η = viscosity, λ = relaxation time, and $\dot{\gamma}$ = shear rate.

Notations

$C_{\mathrm{p}}^{\mathrm{m}}$ = specific heat capacity of the melt, J·kg^{-1}·K^{-1}
$C_{\mathrm{p}}^{\mathrm{b}}$ = specific heat capacity of the barrel, J·kg^{-1}·K^{-1}
$C_{\mathrm{p}}^{\mathrm{s}}$ = specific heat capacity of the screw, J·kg^{-1}·K^{-1}
e_i = distance between reactors i and $i + 1$, m
E = activation energy, J·mol^{-1}
f_i = filling ratio for reactor i
F_0 = inlet mass flow rate, kg·s^{-1}
$F_{\mathrm{d}i}$ = direct mass flow rate, kg·s^{-1}
F_{i-1} = mass flow rate coming from the $(i - 1)$th reactor
F_{i+1} = mass flow rate coming from the $(i + 1)$th reactor
$F_{\mathrm{p}i}$ = Poiseuille flow rate produced by reactor i, kg·s^{-1}
F_{ri} = reverse flow rate produced by reactor i, kg·s^{-1}
I_0 = inlet initiator concentration, mol·m^{-3}
k = kinetic constant, s^{-1}
$K_{\mathrm{d}i}$ = geometric constant
K_{ri} = geometric constant
M_0 = inlet monomer concentration, mol·m^{-3}
$\mathscr{M}$ = molar mass of the polymer, kg·mol^{-1}
$\mathscr{M}^{\mathrm{I}}$ = molar mass of the initiator, kg·mol^{-1}
$\mathscr{M}^{\epsilon}$ = molar mass of the monomer
M_i^{m} = mass of the melt in the completely filled ith reactor, kg
M_i^{b} = mass of the barrel in the ith section, kg
M_i^{s} = mass of the screw in the ith section, kg
n_i^{I} = mole number of the initiator, mol
n_i^{ϵ} = mole number of the monomer, mol
N = rotation speed, rpm
P_{a} = atmospheric pressure, Pa
P_i = ith reactor pressure, Pa
r_i = reaction rate in reactor i, mol·s^{-1}·m^{-3}
R = ideal gas constant, J·mol^{-1}·K^{-1}
s^{b} = transversal section of the barrel, m^2
s^{s} = transversal section of the screw, m^2
S_{b} = contact surface between the melt and the barrel, m^2
S_{e} = contact surface between the surroundings and the barrel, m^2
S_{s} = contact surface between the melt and the screw, m^2
t = time, s
T_i^{m} = temperature of the melt in reactor i, K

T_i^b = temperature of the piece of barrel associated with reactor i, K
T_i^s = temperature of the piece of screw associated with reactor i, K
V_i = volume of reactor i, m^3
w_i^I = mass fraction of the initiator
w_i^ϵ = mass fraction of the monomer

Subscripts or Superscripts

b = barrel
i = reactor number
m = melt
s = screw

Greek Letters

α = constant appearing in the reaction rate
α_e = convective heat-transfer coefficient with the ambient air, $W \cdot m^{-2} \cdot K^{-1}$
α_b = convective heat-transfer coefficient between the barrel and the melt, $W \cdot m^{-2} \cdot K^{-1}$
α_s = convective heat-transfer coefficient of the screw and the melt, $W \cdot m^{-2} \cdot K^{-1}$
λ_b = thermal conductivity of the barrel, $W \cdot m^{-1} \cdot K^{-1}$
λ_s = thermal conductivity of the screw, $W \cdot m^{-1} \cdot K^{-1}$
Ψ_i = viscous heat dissipation in reactor i, W
ΔH = reaction enthalpy, $J \cdot mol^{-1}$
Φ_i = heat flux due to electrical resistance heaters in reactor i, W
ρ = polymer density, $kg \cdot m^3$
η_i = melt viscosity in reactor i, Pa·s

Literature Cited

(1) Haley, T. A.; Mulvaney, S. J. On-line system identification and control design of an extrusion cooking process: Part ii. model predictive and inferential control design. *Food Control* **2000**, *11* (2), 121−129.

(2) Tan, J.; Hofer, J. M. Self-tuning predictive control of processing temperature for food extrusion. *J. Process Control* **1995**, *5* (3), 183−189.

(3) Van Antwerp, J. G.; Featherstone, A. P.; Braatz, R. D. Robust cross-directional control of large scale sheet and film processes. *J. Process Control* **2001**, *11* (2), 149−177.

(4) Elsey, J.; Riepenhausen, J.; McKay, B.; Barton, G. W.; Willis, M. Modeling control of a food extrusion process. *Comput. Chem. Eng.* **1997**, *21*, S361−S366.

(5) Wang, L.; Chessari, C.; Karpiel, E. Inferential control of product quality attributes-application to food cooking extrusion process. *J. Process Control* **2001**, *11* (6), 621−636.

(6) Choulak, S.; Couenne, F.; Thomas, G.; Cassagnau, P.; Michel, A. Methodology for robust control of pressure for ϵ-caprolactone polymerization in a twin screw extruder. *Chimia* **2001**, *55* (3), 244−246.

(7) Vergnes, B.; Della Valle, G.; Delamare, L. Global computer software for polymer flows in corotating twin screw extruders. *Polym. Eng. Sci.* **1998**, *38* (11), 1781−1792.

(8) Tayeb, J.; Vergnes, B.; Della Valle, G. A basic model for a twin screw extruder. *J. Food Sci.* **1989**, *54*, 1047−1056.

(9) Poulesquen, A. Contribution à la modélisation de l'extrusion réactive en machine bi-vis. Ph.D. Thesis, Ecole des Mines de Paris, Paris, Dec 2001.

(10) Poulesquen, A.; Vergnes, B.; Cassagnau, Ph.; Gimenez, J.; Michel, A. Polymerization of ϵ-caprolactone in a twin screw extruder: Experimental study and modelling. *Int. Polym. Process.* **2001**, *16* (1), 31−38.

(11) Poulesquen, A.; Vergnes, B. A study of residence time distribution in co-rotating twin screw extruders: Part i: theoretical modelling. *Polym. Eng. Sci.* **2004**, *43* (12), 1841−1848.

(12) Poulesquen, A. Vergnes, B.; Cassagnau, Ph.; Michel, A.; Carneiro, O. S.; Covas, J. A. A study of residence time distribution in co-rotating twin screw extruders: Part ii: Experimental validation. *Polym. Eng. Sci.* **2004**, *43* (12), 1849−1862.

(13) Ganzeveld, K. J.; Capel, J. E.; Van Der Wal, D. J.; Janssen, L. P. B. M. The modelling of counter-rotating twin screw extruders as reactors for single-component reactions. *Chem. Eng. Sci.* **1994**, *49* (10), 1639−1649.

(14) De Graaf, R. A.; Rohde, M.; Janssen, L. P. B. M. A novel model predicting the residence-time distribution during reactive extrusion. *Chem. Eng. Sci.* **1997**, *52* (23), 4345−4356.

(15) Yacu, W. A. Modeling a twin screw co-rotating extruder. *J. Food Eng.* **1985**, *8*, 1−21.

(16) Kulshreshtha, M. K.; Zaror, C. A.; Jukes, J.; Pyle, D. L. A generalized steady-state model for twin screw extruders. *Trans. Inst. Chem. Eng.* **1991**, *69* (C), 189−199.

(17) Kulshreshtha, M. K.; Zaror, C. A. An unsteady-state model for twin screw extruders. *Trans. Inst. Chem. Eng.* **1992**, *70* (C), 21−28.

(18) Li, C. H. Modelling extrusion cooking unsteady. *Math. Comput. Model.* **2001**, *33*, 553−563.

(19) Agassant, J. F.; Avenas, P.; Sergent, J. P.; Vergnes, B.; Vincent, M. *La mise en forme des matières plastiques*; Technique et Documentation Lavoisier: Paris, 1996.

(20) Booy, M. L. Isothermal flow of viscous liquids in corotating twin screw devices. *Polym. Eng. Sci.* **1980**, *20* (18), 1220−1228.

(21) Domschke, T.; Justus, C. Heat transfer in single and twin screw extruders. *Int. Polym. Process.* **1993**, *VIII* (4), 294−307.

(22) Gimenez, J. Polymerisation de l'epsilon-caprolactone en extrudeuse: études cinétiques et rhéologiques en vue du controle du procédé. Ph.D. Thesis, Claude Bernard University, Lyon, France, 1999.

(23) Gimenez, J.; Cassagnau, P.; Michel, A. Bulk polymerization of caprolactone in twin scew extruder: A step toward the process control. *Int. Polym. Process.* **2000**, *15* (1), 20−27.

(24) Gimenez, J.; Cassagnau, P.; Michel, A. Bulk polymerization of ϵ-caprolactone: rheological predictive laws. *J. Rheol.* **2000**, *44* (3), 527−547.

Received for review December 9, 2003
Revised manuscript received September 2, 2004
Accepted September 3, 2004

IE0342964